Anisotropic Exchange Effects in Temperature and Pressure Dependences of EPR Zero-Field Splitting in $[(C_6H_5)_3(n\text{-propyl})P]_2Cu_2Cl_6$

D. Gatteschi*

Dipartamento di Chimica, Universita di Firenze, v. Maragliano 75/77, Firenze, Italy

J. Goslar, W. Hilczer, and S. K. Hoffmann*

Institute of Molecular Physics, Polish Academy of Sciences, Smoluchowskiego 17, PL-60179 Poznań, Poland

C. Zanchini

Dipartamento di Chimica, Universita della Calabria, Arcavacata di Rende (Cosenza), Italy

Received June 28, 1995[⊗]

X-band single-crystal and powder EPR data were collected in the temperature range 4.2−300 K and under hydrostatic pressure up to 500 MPa for $[(C_6H_5)_3(n\text{-propyl})P]_2Cu_2Cl_6$ ($C_{42}H_{44}P_2Cu_2Cl_6$). The crystal and molecular structure have been determined from X-ray diffraction. The compound crystallizes in the monoclinic space group $P2_1/n$ ($Z = 2$) and have unit cell dimensions of $a = 9.556(5)$ Å, $b = 17.113(3)$ Å, $c = 13.523(7)$ Å, and $\beta = 96.10(4)°$. The structure consists of two controsymmetric $Cu_2Cl_6^{2-}$ dimers well separated by complex anions. EPR spectra are typical for the triplet $S = 1$ state of $Cu_2Cl_6^{2-}$ dimer with parameters $g_x = 2.114(8)$, $g_y = 2.095(8)$, $g_z = 2.300(8)$, and $D_x = 0.025(1)$ cm^{-1}, $D_y = 0.057(1)$ cm^{-1}, and $D_z = -0.082(1)$ cm^{-1} at room temperature. The **D** tensor is dominated by a contribution from anisotropic exchange but the dipole−dipole Cu−Cu coupling is not much less. The anisotropic exchange integrals were estimated to be as follows: $J_{xy,x^2-y^2}{}^{an} = -45$ cm^{-1}, $J_{xy,xy}{}^{an} = +17$ cm^{-1}, $J_{xy,yz}{}^{an} = +62$ cm^{-1}. The **D** tensor components are strongly temperature dependent and linearly increase on cooling with an anomalous nonlinear behavior below 100 K. The D values increase linearly with pressure, but the effect is much smaller than the temperature effect. This suggests that the **D** *vs T* dependence is dynamical in origin. EPR data, a possible mechanism, and contributions to the observed dependences are discussed and compared to EPR results for similar compounds.

Introduction

Compounds of the type $A_2Cu_2Cl_6$ containing $Cu_2Cl_6^{2-}$ dimers have been extensively studied in the last several years to determine magnetostructural correlation covering a wide range of structural parameters.[1−4] The geometry of these dimers in all cases has been found to be either planar, bifold, or twisted. In the first two cases, the $Cu_2Cl_6^{2-}$ dimers are stacked in a crystal and the dimer geometry is stabilized by interactions with countercations A. The twisted dimers occur in the crystal with large cations A having little or no hydrogen-bonding capabilities, and the actual $Cu_2Cl_6^{2-}$ geometry results from an interplay between lattice forces and a tendency to lowering chlorine−chlorine repulsion energy within $Cu_2Cl_6^{2-}$ pseudotetrahedra.

Besides the well-known dependence of the intradimer exchange coupling of the Cu−Cl−Cu bridge angle and length, the coupling was found to be strongly affected by a degree of bifold or twisted distortions. In planar $Cu_2Cl_6^{2-}$ dimers copper(II) ions are antiferromagnetically coupled. For a small bifold angle between the central Cu_2Cl_2 plane and the terminal $CuCl_2$ plane, the exchange coupling is antiferromagnetic but becomes ferromagnetic for bifold angles larger than 25°.[3] In twisted geometry the exchange coupling is ferromagnetic for twist angles between bridging plane Cu_2Cl_2 and the terminal $CuCl_2$ plane, in the range from 40 to about 85°.[3]

A number of spectral data are available on chlorocuprates with $Cu_2Cl_6^{2-}$ dimers, including optical and EPR data.[5−9] Theoretical calculations of the electronic structure and exchange coupling constant J with the SCF−Xα−SW method for a model $Cu_2Cl_6^{2-}$ dimer[10] show a good agreement between observed and calculated electronic d−d transitions and dimer charge-transfer bands, and reproduced qualitatively the observed variations of J value with the degree of tetrahedral distortion. Variational CI calculations have been recently published, where comparisons between the calculated singlet−triplet energy gaps using different theoretical methods are reported.[11,12]

In our previous paper[13,14] we reported EPR single crystal measurements in chlorocuprates $[(C_6H_5)_3(n\text{-propyl})A]_2Cu_2Cl_6$

[⊗] Abstract published in *Advance ACS Abstracts,* January 15, 1996.

(1) Willett, R. D. In *Magneto-Structural Correlations in Exchange Coupled Systems*; Willett, R. D., Gatteschi, D.; Kahn, O., Eds.; NATO ASI Series; Reidel: Dordrecht, The Netherlands, 1985; p 389.
(2) O'Brian, S.; Gaura, R. M.; Landee, C. P.; Ramakhrishna, B. L.; Willett, R. D. *Inorg. Chim. Acta* **1988**,*141*, 83.
(3) Scott, B.; Willett, R. D. *Inorg. Chim. Acta* **1988**, *141*, 193.
(4) Blanchette, J. T.; Willett, R. D. *Inorg. Chem.* **1988**, *27*, 843.
(5) Textor, M.; Dubler, E.; Oswald, H. E. *Inorg. Chem.* **1974**, *13*, 1361.
(6) Willett, R. D.; Liles, D. L.; Michelson, C. *Inorg. Chem.* **1967**, *6*, 1885.
(7) Chow, C.; Willett, R. D. *J. Chem. Phys.* **1973**, *59*, 5903.
(8) Desjardins, S. R.; Wilcox, D. E.; Musselman, R. L.; Solomon, E. I. *Inorg. Chem.* **1987**, *26*, 288.
(9) Scott, B.; Geiser, U.; Willett, R. D.; Ptyal, B.; Landee, C. P.; Greeney, R. E.; Manfredini, T.; Pellacani, G. C.; Corradi, A. B.; Battaglia, L. P. *Inorg. Chem.* **1988**, *27*, 2454.
(10) Bencini, A.; Gatteschi, D. *J. Am. Chem. Soc.* **1986**, *108*, 5763.
(11) Miralles, J.; Dauday, J. P.; Caballol, R. *Chem. Phys. Lett.* **1992**, *198*, 555.
(12) Castell, O.; Miralles, J.; Caballol, R. *Chem. Phys.* **1994**, *179*, 377.
(13) Bencini, A.; Gatteschi, D.; Zanchini, C. *Inorg. Chem.* **1985**, *24*, 704.

0020-1669/96/1335-1148$12.00/0

Table 1. Crystal and Data Collection Parameters for $[(C_6H_5)_3(n\text{-propyl})P]_2Cu_2Cl_6$

formula	$C_{42}H_{44}P_2Cu_2Cl_6$
fw, g mol^{-1}	950.57
cryst syst	monoclinic
space group	$P2_1/n$
a, Å	9.556(5)
b, Å	17.113(3)
c, Å	96.10(4)
β, deg	96.10(4)
V, Å	2199
Z	2
d_{calc}, g cm^{-3}	1.436
T, °C	20
λ, Å	0.7107 (Mo Kα)
collcn range	$\pm h,k,l$ ($2\theta < 48°$)
R[a]	0.042
Rw[b]	0.042

[a] $R = \sum||F_o| - |F_c||/\sum|F_o|$. [b] $[\sum w(|F_o| - |F_c|)^2/\sum w(|F_o|)^2]^{1/2}h$.

(A = P, As, Sb in the following indicated as *p*, *as*, *sb* respectively) and the influence of temperature on the EPR spectra. The compounds show the twisted geometry of centrosymmetric $Cu_2Cl_6^{2-}$ dimers with twist angles 50.0(2), 48.2(2), and 44.4(2)° for *p*, *as*, and *sb* respectively. Copper(II) ions are ferromagnetically coupled with J values equal to −80(9) cm^{-1}, −39 cm^{-1} (error not reported), and −90(14), for *p*,[15] *as*,[15,16] and *sb*,[15] respectively, using the spin hamiltonian $H = J\mathbf{S}_1\cdot\mathbf{S}_2$. The J value is indicative of the strength of exchange interaction between the ground states of the Cu(II) ions. The anisotropic exchange coupling contributes to the zero-field splitting **D** tensor measured by the EPR spectra. We found that in the *p*, *as*, and *sb* compounds this contribution is in excess of the contribution to the **D** tensor from direct dipole−dipole magnetic interaction. It appeared, moreover, that **D** splitting was strongly temperature dependent and increased linearly on cooling.[14]

Since the Cu_2Cl_2 bridge geometry is not expected to be significantly affected by temperature, the dipole−dipole coupling contribution to **D** can be assumed as a negligibly temperature dependent, so we have interpreted **D** tensor temperature dependence as due to a variations in anisotropic exchange coupling. Surprisingly, the **D** tensor was not affected by hydrostatic pressure up to 300 MPa indicating that *D vs T* dependence is dynamical in origin. We attributed it to changes in population of vibronic levels, which are characterized by different anisotropic exchange integral, appearing when tetrahedral deformation dynamically increases on heating. Recently, the 113 K structure determination for *as* was carried out[17] in order to see if significant structural differences exist between room and low temperature as suggested by EPR data.[13] The results show rather small structural changes, the largest being for the bridge Cu−Cl(2) length which increases from 2.316(2) Å at room temperature to 2.327(2) Å at 113 K, with a simultaneous increase in tetrahedral angle from 145.2(1) to 146.3(1)°. These changes seem to be very small, and the question is if they are large enough to explain the observed variations in EPR parameters or if these variations are pure vibrational in origin and go without significant modification in $CuCl_4$ tetrahedron geometry.

In order to make an additional contribution in this field, we performed detailed studies on a very similar compound containing $Cu_2Cl_6^{2-}$ dimers, *i.e.* $[(C_6H_5)_3(n\text{-propyl})P]_2Cu_2Cl_6$ (in the following indicated as (*n-pr*)*p*) which exhibits a larger zero-field splitting value and the largest EPR temperature variations among $A_2Cu_2Cl_6$ compounds studied so far.

Table 2. Positional Parameters for Non-Hydrogen Atoms[a] and Equivalent Isotropic Thermal Parameters[b,c] (Esd's in Parentheses) for $[(C_6H_5)_3(n\text{-propyl})P]_2Cu_2Cl_6$

atom	x	y	z	U(eq), Å^2
Cu	2094(6)	3099(4)	11859(5)	65.2(4)
P	−604(1)	4225(1)	2049(1)	52.7(7)
Cl(1)	451(2)	−356(1)	2579(1)	86(1)
Cl(2)	1202(1)	−624(1)	237(1)	80(1)
Cl(3)	341(1)	1489(1)	1841(1)	88(1)
C(1)	1026(5)	3772(3)	1823(3)	59(3)
C(2)	1362(6)	3807(4)	742(4)	83(4)
C(3)	2686(6)	3380(4)	579(5)	103(5)
C(4)	−476(5)	5266(3)	2028(3)	54(3)
C(5)	781(5)	5647(3)	1900(3)	61(3)
C(6)	847(6)	6458(3)	1956(4)	72(4)
C(7)	−302(6)	6880(3)	2141(4)	74(4)
C(8)	−1544(6)	6512(3)	2268(4)	78(4)
C(9)	−1652(5)	5708(3)	2222(3)	64(3)
C(10)	−1935(5)	3872(3)	1131(3)	54(3)
C(11)	−2017(6)	3063(3)	986(4)	72(4)
C(12)	−2955(6)	2756(4)	251(4)	84(4)
C(13)	−3825(6)	3230(4)	−344(4)	81(4)
C(14)	−3748(6)	4022(4)	−218(4)	75(5)
C(15)	−2809(5)	4345(3)	516(4)	63(3)
C(16)	−1006(5)	3963(3)	3267(3)	54(3)
C(17)	−2323(5)	3697(3)	3441(4)	64(3)
C(18)	−2616(6)	3559(3)	4408(4)	79(4)
C(19)	−1603(7)	3684(3)	5188(4)	80(5)
C(20)	−307(7)	3944(3)	5024(4)	80(5)
C(21)	16(6)	4087(3)	4060(4)	69(4)

[a] Coordinates multiplied by 10^4 (Cu 10^5). [b] U(eq) = $^1/_3$ of the trace of the orthogonalized $\mathbf{U}_{ij}$. [c] Thermal parameters multiplied by 10^3.

Experimental Section

X-ray Data Collection and Reduction. X-ray data for (*n-pr*)*p* were collected on an Enraf-Nonius CAD-4 four-circle diffractometer with Mo Kα radiation. The data were collected from a trigonal prism shaped crystal having approximate dimensions 0.6 × 0.39 × 0.06 mm. Accurate unit cell parameters were derived from least squares refinement of the setting angles of 25 reflections with $8° < \theta < 15°$. Details of the crystal data and data collections are listed in Table 1. No systematic variation of intensity of three standard reflections measured every 120 min was observed. The principal computer programs used in the crystallographic calculations are listed in ref 18. The data were corrected for Lorentz and polarization effects[18a] as well as for absorption.[18b] The position of all non-hydrogen atoms were obtained conventional Patterson and Fourier methods using the SHELX-76 package.[18b] The structure were refined with use of a full-matrix least squares method based on minimization of the function $\sum w(|F_o - F_c|)^2$ with weights $w = 1/\sigma(F_o)$. Anisotropic thermal parameters were used for all non-hydrogen atoms. Hydrogen atoms were introduced in calculated positions (C−H =1.08 Å) as fixed contributions to F_c, each with a temperature factor 20% larger than that of the isotropic equivalent of the respective carbon atom. The final R values were $R = 0.042$ and $R_w = 0.042$. The final positional parameters for non-hydrogen atoms are listed in Table 2. The listing of the thermal parameters for the non hydrogen atoms, of the hydrogen atom coordinates are available as Supporting Information.

EPR Measurements. EPR measurements were performed at X-band with two types of spectrometers. At atmospheric pressure a Bruker ESP 380E FT/CW spectrometer was used in CW-mode, and the variable temperature spectra were recorded on single crystals and

(14) Gatteschi, D.; Goslar, J.; Hilczer, W.; Hoffmann, S. K.; Zanchini, C. *Inorg. Chem.* **1989**, *28*, 3395.
(15) Estes, W. E.; Wasson, J. R.; Hall, J. W.; Hatfield, W. E. *Inorg. Chem.* **1978**, *17*, 3657.
(16) Chow, C.; Caputo, R.; Willett, R. D.; Gerstein, B. C. *J. Chem. Phys.* **1974**, *61*, 271.
(17) Scott, B.; Willett, R. D. *Acta Crystallogr., Sect. C* **1991**, *47*, 435.
(18) Stewart, J. M.; Kundall, F. A.; Baldwin, J. C. XRay 72 System of Programs. Technical Report TR 192; University of Maryland: College Park, MD, 1972. (b) Sheldrick, G. SHELX 76 System of Computing Programs. University of Cambridge, England, 1976. (c) Johnson, C. K. *Oak Ridge Natl. Lab., [Rep.] ORNL (U.S.)* **1965**, ORNL-3794.

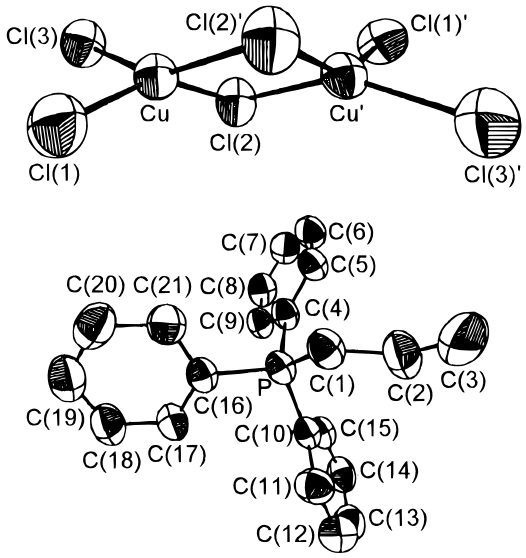

Figure 1. View of the $[Cu_2Cl_6]^{2-}$ and $[(C_6H_5)_3(n\text{-propyl})P]^+$ ions of (*n-pr*)*p* showing thermal ellipsoids.

Table 3. Interatomic Distances (Å) for $[(C_6H_5)_3(n\text{-propyl})P]_2Cu_2Cl_6$ (Esd's in Parentheses)

Distances within $Cu_2Cl_6^{2-}$			
Cu−CI(1)	2.192(2)	Cu−CI(2)'	2.294(2)
Cu−CI(2)	2.315(2)	Cu−Cu	3.361(2)
Cu−CI(3)	2.202(2)		
Distances within $[(C_6H_5)_3(n\text{-propyl})P]^+$			
P−C(1)	1.792(5)	C(10)−C(11)	1.399(7)
P−C(4)	1.787(5)	C(10)−C(15)	1.377(7)
P−C(10)	1.787(5)	C(11)−C(12)	1.371(8)
P−C(16)	1.788(5)	C(12)−C(13)	1.361(9)
C(1)−C(2)	1.531(8)	C(13)−C(14)	1.37(1)
C(2)−C(3)	1.497(9)	C(14)−C(15)	1.380(7)
C(4)−C(5)	1.394(7)	C(16)−C(17)	1.383(7)
C(4)−C(9)	1.402(7)	C(16)−C(21)	1.388(7)
C(5)−C(6)	1.391(7)	C(17)−C(18)	1.387(8)
C(6)−C(7)	1.359(8)	C(18)−C(19)	1.370(8)
C(7)−C(8)	1.370(8)	C(19)−C(20)	1.36(1)
C(8)−C(9)	1.381(7)	C(20)−C(21)	1.393(8)

powders in the temperature range 4.2−300 K using a flow helium cryostat, Oxford CF935. High pressure EPR experiments were performed on a Radiopan SE/X-2544 spectrometer in the temperature range 100−300 K under hydrostatic pressure up to 500 MPa on powder samples. High pressure equipment was described elsewhere.[19] Rotational EPR data were collected in the three orthogonal crystal planes by rotating a crystal around *a*, *b*, and $c^* = a \times b$ crystal axes. The well developed (010) planes and [100] edges allowed us to accurately align the crystal on a goniometer holder under an optical microscope.

Results and Discussion

Description of the Structure of $((C_6H_5)_3(n\text{-propyl})P]_2Cu_2Cl_6$. The crystal structure of *(n-pr)p* consists of $[(C_6H_5)_3(n\text{-propyl})P]^+$ cations and $Cu_2Cl_6^{2-}$ dimeric isolated units. Drawings of the two ions showing the labeling scheme are shown in Figure 1. A list of bond distances and angles are reported in Table 3 and Table 4. The structure *of* (*n-pr*)*p is* very similar to those of the parent $[(C_6H_5)_4X]_2Cu_2Cl_6$ (X = P,[20] As[17] and Sb[13]) compounds, as showed in Table 5, the main differences being the smallest monoclinic angle and the lowest unit cell volume, witness of a more dense crystal packing.

The $[(C_6H_5)_3(n\text{-propyl})P]^+$ cation has the expected tetrahedral configuration around P, with an average C−P−C angle corresponding well to the averaged C−X−C angles (X = P, As, Sb) seen in the $[(C_6H_5)_4X]_2Cu_2Cl_6$ series and with an averaged P−C distance, 1.788 Å, slightly longer than that observed in *p* (Table 3). No systematic deviation of the phenyl rings from a regular hexagon is observed: they are planar within the uncertainty in the positional parameters, the largest deviation being −0.006 Å for C(13).

Table 4. Angles (deg) for $[(C_6H_5)_3(n\text{-propyl})P]_2Cu_2Cl_6$ (Esd's in Parentheses)

Angles within $Cu_2Cl_6^{2-}$			
Cl(2)−Cu−Cl(3)	147.8(1)	Cl(1)−Cu−Cl(2)	96.05(7)
Cl(1)−Cu−Cl(3)	97.71(8)		
Angles within $[(C_6H_5)_3(n\text{-propyl})P]^+$			
C(10)−P−C(16)	110.3(2)	P−C(10)−C(15)	124.3(4)
C(4)−P−C(16)	106.5(2)	P−C(10)−C(11)	117.1(4)
C(4)−P−C(10)	111.7(2)	C(11)−C(10)−C(15)	118.4(5)
C(1)−P−C(16)	109.0(2)	C(10)−C(11)−C(12)	120.2(5)
C(1)−P−C(10)	107.7(2)	C(11)−C(12)−C(13)	120.7(6)
C(1)−P−C(4)	111.6(2)	C(12)−C(13)−C(14)	119.7(6)
P−C(1)−C(2)	114.8(4)	C(13)−C(14)−C(15)	120.5(6)
C(1)−C(2)−C(3)	112.8(5)	C(10)−C(15)−C(14)	120.4(5)
P−C(4)−C(9)	118.6(4)	P−C(16)−C(21)	118.1(4)
P−C(4)−C(5)	121.9(4)	P−C(16)−C(17)	122.0(4)
C(5)−C(4)−C(9)	119.3(4)	C(17)−C(16)−C(21)	119.8(4)
C(4)−C(5)−C(6)	119.7(5)	C(16)−C(17)−C(18)	119.7(5)
C(5)−C(6)−C(7)	120.5(5)	C(17)−C(18)−C(19)	120.2(6)
C(6)−C(7)−C(8)	120.4(5)	C(18)−C(19)−C(20)	120.5(5)
C(7)−C(8)−C(9)	121.0(5)	C(19)−C(20)−C(21)	120.5(6)
C(4)−C(9)−C(8)	119.2(5)	C(16)−C(21)−C(20)	119.3(5)

Table 5. Cu_2Cl_6 Dimer Geometry in $A_2Cu_2Cl_6$ Chlorocuprates

	A			
	$(C_6H_5)_4Sb$	$(C_6H_5)_4As$	$(C_6H_5)_4P$	(n-propyl)$(C_6H_5)_3P$
Cu- - -Cu, Å	3.400	3.382	3.355	3.3615
Cu−Cl(1),[a] Å	2.336	2.333	2.321	2.315
Cu−Cl(2),[a] Å	2.290	2.305	2.292	2.294
θ,[b] deg	94.6	93.7	93.3	
α,[c] deg	44.4	48.2	50.0	45.0
β_1,[d] deg	147.9	145.2	143.6	147.8
β_2,[d] deg	147.4	144.6	143.3	147.3
J,[e] cm^{-1}	90(14)	39	80(9)	93(11)
ref	13	17	20	this work

[a] Bridging chlorides. [b] Cu−Cl−Cu bridge angle. [c] Dihedral angle (twist angle). [d] Trans Cl−Cu−Cl angles in $CuCl_4$ tetrahedra. [e] For Hamiltonian $H = J\mathbf{S}_1\cdot\mathbf{S}_2$, data from ref 15.

The $Cu_2Cl_6^{2-}$ anion geometry is substantially identical in all the chlorocuprates compounds[13,17,20] which structure we are comparing (Table 5), with a Cl−Cu−Cl bridging angle of about 94° and nearly equal bridge arms ($\Delta \approx 0.03$ Å), as shown in Table 3. The Cu−Cu distance for (*n-pr*)*p*, 3.361(2) Å, compares well with that of 3.355(1) Å observed in *p*.[20] In the present complex the distances to the terminal chlorine atoms, 2.192(2) and 2.202(2) Å, are different from each other, but their difference, $\Delta \approx 0.01$ Å, is the smallest observed in the series of the homologous compounds. A characteristic feature of the compounds is that the tetrahedra $CuCl_4^{2-}$ forming the dimeric structure are strongly distorted toward the planar geometry with the flattening angle of about $\beta/2 \approx 74°$ in approximately D_{2d} symmetry or with a dihedral angle of a $\alpha \approx 45°$ if an approximate C_{2v} distorted tetrahedron is considered to describe the coordination environment of the copper ion.

EPR Spectra. Powder and single-crystal EPR spectra are typical for a triplet state of $Cu_2Cl_6^{2-}$ dimers with zero-field splitting lower than the resonance frequency and relative strong $\Delta M_s = \pm 2$ forbidden transition signal at about $g = 4$ position. Single-crystal EPR lines are rather broad with a peak-to-peak value varying with angle in the range from 19 to about 40 mT. Relatively large ΔB_{pp} values and the overlap of the lines limit

(19) Stankowski, J; Gałęzewski, A.; Krupski, M.; Waplak, S.; Gierszal, H. *Rev. Sci. Instrum.* **1976**, *47*,128.
(20) Qui, D. T.; Daoud, A.; Mhiri, T. *Acta Crystallogr., Sect. C* **1989**, *45*, 33.

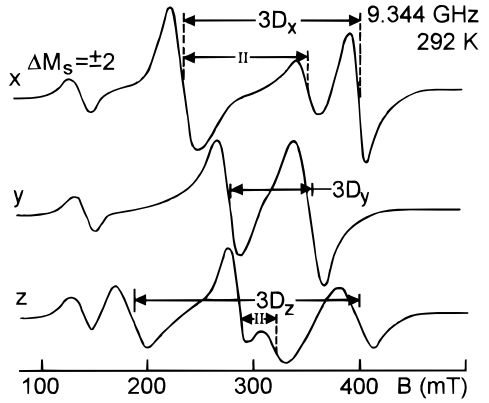

Figure 2. Room temperature single-crystal EPR spectra of (*n-pr*)*p* along principal **D** tensor axes of one of the two magnetically nonequivalent $[Cu_2Cl_6]^{2-}$ ion (dimer I). The dimer II lines are marked.

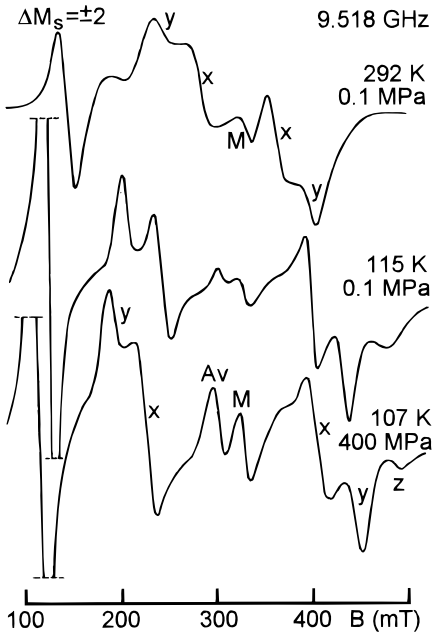

Figure 3. Polycrystalline powder EPR spectra of (*n-pr*)*p* recorded at different temperature and hydrostatic pressures. The lines along the principal **D** tensor directions are marked by *x*, *y*, and *z*. The lines indicated with Av and M are due to impurities.

the accuracy of EPR parameters measurements. Single-crystal EPR spectra recorded at room temperature along the principal axes of the **D** and **g** tensors are shown in Figure 2.

The spectra are temperature and pressure dependent with zero-field splitting increasing with lowering temperature or increasing pressure. The line width decreases on cooling in all crystal orientations, but the line narrowing is *ca*. 10% of the initial value. The ΔB_{pp} value can be related to a phonon modulation of the exchange anisotropy which is known to lead to a linear temperature dependence proportional to $(\Delta g)^2 J^4$.[21] The temperature and pressure effects in powder EPR spectra are shown in Figure 3, where the spectral peaks from **D** tensor *x*, *y*, and *z* axes are marked. A strong temperature influence on the crystal EPR spectrum is observed when magnetic field is roughly parallel to the Cu−Cu direction *i.e.* in the *c*b* plane at about $\theta = 15°$. At room temperature the fine structure doublet is observed in this orientation. When the temperature is lowered, the doublet lines split. The splitting increases on cooling nearly linearly down to about 150 K, then non-linearity appears, and the dependence saturates below 20 K (Figure 4).

The experimental angular dependence of the resonance field in the three orthogonal crystal planes is shown by points in

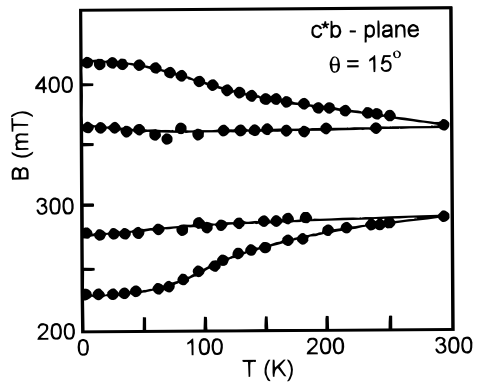

Figure 4. Temperature variations of the resonance fields of the single crystal EPR lines of (*n-pr*)*p* for magnetic field in the *c*b* plane at $\theta = 15°$ from the *b* axis.

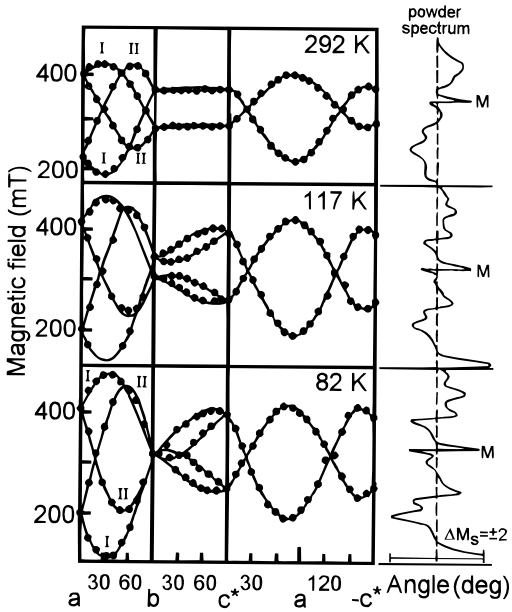

Figure 5. Experimental (point) and calculated (solid lines) angular variation of the resonance fields at (upper) 292 K and 9.764 GHz, (middle) 117 K and 9.829 GHz, and (lower) 82 K and 9.841 GHz for (*n-pr*)*p*. I and II indicate the two inequivalent dimers in the unit cell. On the right side the corresponding powder EPR spectra are reported. M is due to an impurity.

Figure 5. The dependence is presented for room temperature and for two lower temperatures where the largest changes of the spectral parameters were observed. The solid curve were calculated using an iterative computer procedure.[22] The splitting between the lines in powder spectra were taken as initial parameters of the procedure and the **D** tensor was assumed to be traceless. The powder spectra are plotted on the right side of the angular dependences (Figure 5). The calculated **g** and **D** principal values and directions are collected in Table 6. The **g** and **D** tensors are not axial and have collinear principal axes. The *z*-axis lies close to the *ab* plane along the direction of the tetrahedral compression of the $CuCl_4^{2-}$ moiety. The *z*-axis direction is affected by the temperature. The *x*-axis, along which the minimal zero-field splitting is observed, lies in the *c*b* plane at $\theta = 18°$, *i.e.* exactly along the Cu−Cu direction, and is temperature independent. The temperature changes of the angular dependence presented in Figure 5 are mainly due to variation in the **D** tensor components and, to a lower extent, to

(21) Kite, T. M.; Drumheller, J. E.; Emerson, J. E. *J. Magn. Reson.* **1982**, *68*, 20.
(22) Buluggiu, E.;, Vera, A. *J. Magn. Reson.* **1980**, *41*,195.

Table 6. Principal Values and Directions of **g** and **D** Tensors for (*n-pr*)*p* at 292, 117, and 82 K[a]

T (K)	*g*	*D* (in cm^{-1})	direction cosines		
292	$g_x = 2.114(8)$	$D_x = 0.025(1)$	0.0000	±0.3123	±0.9500
	$g_y = 2.095(8)$	$D_y = 0.057(1)$	±0.4421	±0.8521	±0.2801
	$g_z = 2.300(8)$	$D_z = -0.082(1)$	±0.8970	±0.4200	±0.1380
117	$g_x = 2.140(8)$	$D_x = 0.051(2)$	0.0000	±0.3123	±0.9500
	$g_y = 2.110(8)$	$D_y = 0.075(2)$	±0.5263	±0.8078	±0.2656
	$g_z = 3.370(8)$	$D_z = -0.126(2)$	±0.8503	±0.5000	±0.1643
82	$g_x = 2.155(8)$	$D_x = 0.061(1)$	0.0000	±0.3123	±0.9500
	$g_y = 2.110(8)$	$D_y = 0.081(1)$	±0.5684	±0.7816	±0.2569
	$g_z = 3.380(8)$	$D_z = -0.124(1)$	±0.5400	±0.5400	±0.1775

[a] The direction cosines are given with respect to the *abc** reference frame.

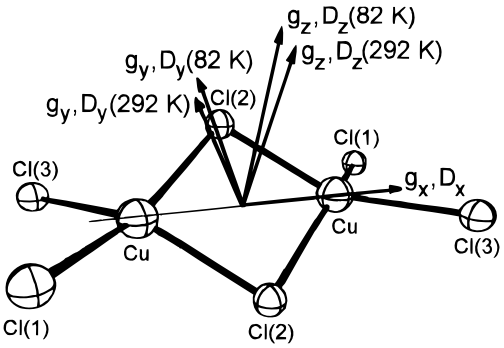

Figure 6. Sketch of the $Cu_2Cl_6^{2-}$ anion in (*n-pr*)*p* with **D** and **g** tensor principal directions at 292 and 82 K.

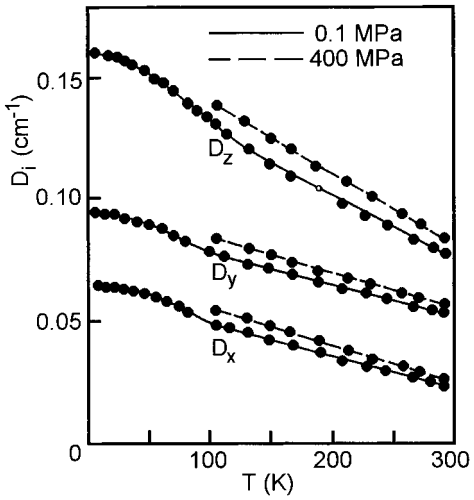

Figure 7. Temperature dependence of the **D** tensor principal values under atmospheric pressure 0.1 MPa and high hydrostatic pressure 400 MPa for (*n-pr*)p. High pressure data were obtained from polycrystalline powder EPR measurements.

the temperature variations of the **g** tensor and principal axes directions. All the **D** and **g** tensors components increase on cooling but **D** remains nonaxial, whereas the nonaxiality of **g** increases. Lowering the temperature results also in a rotation of the principal axes system around the *x*-axis in such a way that the *z*-axis, forming an angle of 26° with a at 292 K, inclines to 35° at 82 K and then becomes practically temperature independent. The *x*, *y*, and *z* axis of the **g** and **D** tensors at 292 K and 82 K are drawn in Figure 6.

Temperature variations of the principal **D** values are shown in Figure 7 for atmospheric and high hydrostatic pressure. The increasing pressure induces a linear increase of the **D** values, as is shown in Figure 8. The changes are much smaller than

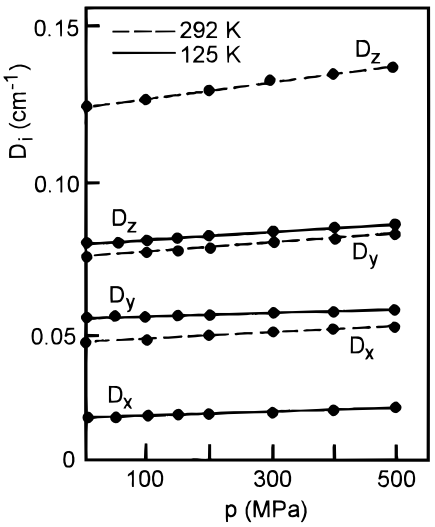

Figure 8. Pressure dependence of the **D** tensor principal values at 292 and 125 K for (*n-pr*)*p*.

those produced by the temperature, but an increase in pressure acts as a decrease in temperature.

The similarity in the structures at room temperature suggests that also low temperature structures can be very similar. However, as previously discussed, the 113 K crystallographic data for *as*[17] indicate that temperature influence on the structure is not substantial and thermal lattice contraction is rather small and does not affect the dimer moiety (Table 5). The magnetic properties of the compounds are also very similar[15,16] with a relatively strong ferromagnetic exchange interaction between the two copper(II) ranging from -46 cm^{-1} (error not reported)[16] to $-93(11)$ cm^{-1} for (*n-pr*)*p*. Because of a strong correlations of *J* and *g* values in the case of ferromagnetic coupling during the fit of the magnetic susceptibility data,[16] the uncertainties on *J* are quite large, and it should be concluded that the isotropic coupling constants have similar ferromagnetic values in this group of chlorocuprates.

The *g* factors *in* (*n-pr*)*p* indicate a $|xy\rangle$ or $|x^2 - y^2\rangle$ ground state for the copper(II) ions as expected for D_{2d} or C_{2v} distorted tetrahedron,[23] respectively. The principal axes of the **g** and **D** tensors coincide also in *as*,[7] whereas a noncoincidence of the *x*- and *y*-axes was found in *p* and *sb*;[13] however, in all the compounds the *z*-axis lies along the compression axis of $CuCl_4^{2-}$ tetrahedron and a perpendicular component is parallel to the Cu−Cu direction, as expected for a centrosymmetric dimer. The *g* factor and the zero field splitting values are very similar in all the compounds indicating that electronic structure of the dimeric units are not significantly altered by the different counterions.

The zero-field splitting tensor in binuclear copper(II) complexes is expected to have contributions from dipole−dipole magnetic interaction and from anisotropic exchange

$$\mathbf{D} = \mathbf{D}^{dip} + \mathbf{D}^{ex}$$

The maximal splitting from $\mathbf{D}^{dip}$ is expected along the Cu−Cu direction. In our case, however, the largest component of **D** is D_z, and this means that anisotropic exchange dominates over the dipolar contribution. When the **g** tensors of the two copper(II) ions are collinear, the dipolar contribution (in cm^{-1}) can be calculated as

$$D_i^{dip} = 0.325 g_i^2 r^{-3}(1 - 3\cos^2\theta)$$

where *r* is the Cu−Cu distance (in Å), g_i is the *g* value along

(23) Hoffmann, S. K.; Goslar, J. *J. Solid State Chem.* **1982**, *44*, 343.

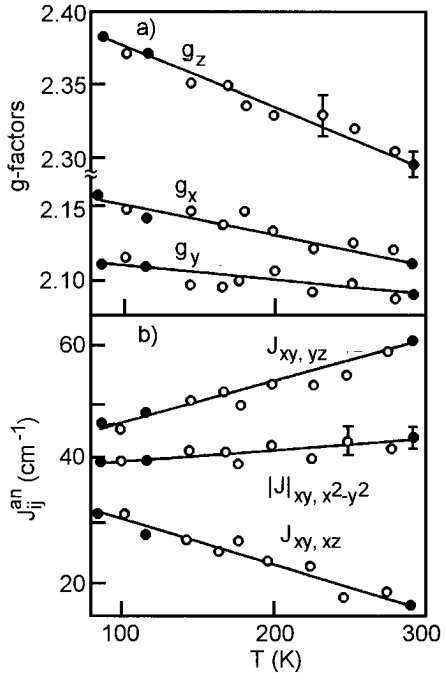

Figure 9. (a) Temperature dependence of the *g* factors determined from single crystal (full circles) and powder (open circles) EPR spectra. (b) Temperature dependence of anisotropic exchange integrals for (*n-pr*)*p*.

the magnetic field, and θ is the angle between the **r** vector and the direction of the magnetic field. In (*n-pr*)*p*, where $r = 3.36$ Å, we can calculate the $\mathbf{D}^{dip}$ components, and using the experimental **D** room temperature values, we obtain the $\mathbf{D}^{ex}$ tensor and its principal values. In centrosymmetric dimeric units no contribution due to antisymmetric exchange is expected, and the $\mathbf{D}^{ex}$ components can be related to the *g* factor anisotropy Δg and to the anisotropic exchange coupling constant J_{ij}^{an} between the ground state $|i\rangle$ on one copper(II) ion and the excited $|j\rangle$ state on the other according to

$$D_x^{ex} = \frac{1}{8}\Delta g_x^2 J_{xy,yz}^{an} \qquad D_y^{ex} = \frac{1}{8}\Delta g_y^2 J_{xy,xz}^{an}$$

$$D_z^{ex} = \frac{1}{32}\Delta g_z^2 J_{xy,x^2-y^2}^{an} \qquad (1)$$

where a $|xy\rangle$ ground state is assumed. From D_i^{ex} and the experimental $\Delta g_i = g_i - 2.0023$ values we can evaluate $J_{xy,yz}^{an} = 62(5)$ cm^{-1}, $J_{xy,xz}^{an} = 17(5)$ cm^{-1}, and $J_{xy,x^2-y^2}^{an} = -45(5)$ cm^{-1} at room temperature. The calculated values of J_{ij}^{an} are obviously affected by large uncertainty due to the simple procedure followed to obtain them, nevertheless they are clearly indicative that, in (*n-pr*)*p* and, arguing from analogy, in all this group of chlorocuprates, the anisotropic coupling constants are of the same order of magnitude of the isotropic $J_{xy,xy}$ constant.

The zero-field splitting increases when the temperature is lowered (Figure 7). We attribute this to temperature variations of the anisotropic exchange since the dipolar coupling seems to be less temperature sensitive. Two effects results in $\mathbf{D}^{ex}$ *vs T* dependence: temperature variations of the **g** tensor and temperature changes in the J_{ij}^{an} integrals. For a separation of these two contributions a knowledge of the *g* factor temperature dependence is needed. We known it at low accuracy since our *g* factors are determined with an accuracy of ± 0.004 from single-crystal rotational data and only with an accuracy of ± 0.013 from powder spectra. Thus we can only roughly estimate the two contributions. In the linear region of **D** *vs T* dependence, *i.e.* above approximately 100 K, the *g* values linearly increase on cooling as is shown in Figure 9a. From these dependences and using eq 1, we calculated the temperature variation of J_{ij}^{an} as presented in Figure 9b. It can be observed that the *g* factor temperature dependence is the dominant factor in the **D** *vs T* behavior.

To explain the **g** *vs T* and J_{ij}^{an} *vs T* dependences the following facts should be kept in mind. (1) The dependences are dynamic in origin. This is proven by a very small pressure effect in the present compound and a lack of any pressure effect in *sb*[14] and by the little structural change showed in the X-ray structural investigation of *as*.[17] (2) Despite of a lack of any substantial structural changes the EPR data clearly show that *z*- and *y*-axes of the **D** and **g** tensors are affected by temperature. These axes are local crystal field axes and cannot be easily related to the geometry of a distorted tetrahedron. The axes rotation can be a dynamical effect due to anharmonicity of the ligand vibrations in $CuCl_4^{2-}$. (3) Strong vibrational effects are generally observed in $CuCl_4^{2-}$ structures, and optical spectra show a red shift of the d−d and charge transfer bonds on heating.[8,24] (4) It is well documented that exchange coupling is very sensitive to even a small change in dimer bridge geometry, especially for modifications in the bridge angle ϕ.

The J_{ij}^{an} *vs T* dependences show that anisotropic exchange tends to be less anisotropic at low temperatures. But the more characteristic feature is that exchange coupling with the excited $|yz\rangle$ state of the second ion decreases on cooling with a simultaneous increase in the coupling with the $|xz\rangle$ state, whereas the coupling with $|x^2 - y^2\rangle$ is not affected. Such behavior is expected when the bridge angle ϕ increases resulting in an increase in the overlap of the Cu(II) $|xz\rangle$ orbital with chlorine orbital and in a proportional decrease in the overlap of $|yz\rangle$ orbital. The overlap of $|x^2 - y^2\rangle$ is not affected.

The observed temperature effects seems to be even more complicated. The low temperature non linearity of **D** *vs T* can be related to some extent to a depopulation of the excited singlet state since triplet−singlet separation ($J = -93$ (11) cm^{-1}) is relatively large in the present compound and results of the order of vibrational frequencies responsible for the temperature effects in optical spectra of $CuCl_4^{2-}$ complexes.[8,25] A thermal depopulation of vibronic levels characterized by different anisotropic exchange integrals can contribute to the observed J_{ij}^{an} *vs T* dependences. The point dipole approximation can not be perfectly valid because of a delocalization of the unpaired electron on ligands. This delocalization can be temperature dependent, and the $\mathbf{D}^{dip}$ tensor components can vary slowly with temperature, affecting the **D** *vs T* dependence.

Acknowledgment. This work was partially supported by Research Project KBN-2-0979-91-01 of the Polish Committee for Scientific Research.

Supporting Information Available: Listings of thermal parameters for the non-hydrogen atoms and hydrogen atoms coordinates of $[(C_6H_5)_3(n\text{-propyl})P]_2Cu_2Cl_6$ (2 pages). Ordering information is given on any current masthead page.

IC950811H

(24) Mc Donald, R. G.; Hitchman, M. A. *Inorg. Chem.* **1986**, *25*, 3273.
(25) Riley, M. J.; Hitchman, M. A. *Inorg. Chem.* **1987**, *26*, 3205.